Urban Climate 14 (2015) 586–605

Contents lists available at ScienceDirect

Urban Climate

journal homepage: www.elsevier.com/locate/uclim

Vulnerability to heat waves: Impact of urban expansion scenarios on urban heat island and heat stress in Paris (France)

A. Lemonsu [a,*], V. Viguié [b], M. Daniel [a], V. Masson [a]

[a] Météo-France/CNRS, Groupe d'étude de l'atmopshère météorologique, 42 avenue Gaspard Coriolis, 31057 Toulouse cedex, France
[b] Centre international de recherche sur l'environnement et le développement (CIRED), 45 bis avenue de la Belle Gabrielle, F-94736 Nogent sur Marne cedex, France

ARTICLE INFO

Article history:
Received 17 September 2014
Revised 22 September 2015
Accepted 28 October 2015

Keywords:
Urban sprawl
Densification
Urban heat island
Heat wave
Vulnerability indicators
Adaptation to climate change

ABSTRACT

The evolution of heat-wave risk in cities is related to regional climate change in interaction with urban heat island. Land planning and urban transport policies, due to their long-lasting impact on city's size and shape, can also have an influence. However, these combined effects are complex and strongly depend on the indicators used to quantify heat-wave risk. With Paris area as a case study and using an interdisciplinary modelling chain, including a socio-economic model of land-use transport interaction and a physically-based model of urban climate, air temperature in the city during heat waves is simulated for five urban expansion scenarios. The urban heat island is always higher at night and affects preferentially the city centre. Its intensity and spatial extension are moderately impacted by densification process and choice in urban form. But the variation of heat-wave risk with the densification dynamics is not limited to the effect on urban heat island, and also depends on exposure to heat of population. Spatial distribution of population in the city differs according to urban expansion scenarios. The results show that the compact city, by concentrating the inhabitants in areas the most impacted by heat island effect, amplifies the overall vulnerability of population.

1. Introduction

The global warming induced by greenhouse gases emissions is already observed and is going to intensify during the 21st century according to climate projections at the global scale (Meehl and Tebaldi, 2004; Schär et al., 2004; IPCC, 2013). One of the expected consequences is the raise of occurrences of heat waves, that has been highlighted at global and regional scale by numerous studies (Huth et al., 2000; Beniston et al., 2007; Chauvin and Denvil, 2007; Vautard et al., 2007). This issue has for instance been investigated for France by the IMFREX project (Déqué, 2007; Planton et al., 2008), as well as for the Paris region by Lemonsu et al. (2013, 2014). Especially, Lemonsu et al. (2014) indicate that heat waves will become more frequent at the end of the century (at least one event per year), but also they will last longer and will be more intense than today.

These extreme meteorological events are a source of growing concern for cities and urban populations, because high temperatures reached during heat waves are often exacerbated due to urban heat island (UHI) effect (Basara et al., 2010; Tan et al., 2010; Gabriel and Endlicher, 2011; Li and Bou-Zeid, 2013). As a result, there are rising concerns of public and

* Corresponding author.
E-mail addresses: aude.lemonsu@meteo.fr (A. Lemonsu), viguie@centre-cired.fr (V. Viguié), maxime.daniel@meteo.fr (M. Daniel), valery.masson@meteo.fr (V. Masson).

http://dx.doi.org/10.1016/j.uclim.2015.10.007
2212-0955/

institutional stakeholders about the vulnerability of urban areas facing these events (see for instance, Stone and Rodgers, 2001; Solecki et al., 2005; Hamin and Gurran, 2009; Lambert-Habib et al., 2013).

The specificities of urban climate and the resulting UHI are strongly determined by both morphological characteristics and material properties of the urban landscape. Some local-scale action levers are already considered by architects and urban planners for a better thermal regulation of microclimate; for example the use of light-colour materials favoring the reflective properties (Santamouris et al., 2011; Kolokotsa et al., 2013) or the implementation of urban vegetation either ground-based (Potchter et al., 2006; Shashua-Bar et al., 2009) or on building envelope (Harazono et al., 1991; Wong et al., 2003).

In addition, at any given place in the city, the UHI can be impacted by the characteristics of the city as a whole, e.g. its size and shape or the composition and arrangement of the neighbourhoods within it. The choices of urban planning at the scale of a city or of a community of conurbations may consequently play a key role in adaptation strategies (Bass et al., 2003; Rosenzweig et al., 2009; Masson et al., 2013a). The effects of actions led at city-scale, however, may be tricky to understand and evaluate due to the interaction of multi-scale physical processes (i.e. a local action can influence a place far from it due to atmospheric processes) but also of socio-economical mechanisms (i.e. a local action can induce a change in inhabitants behaviours or choices, such as for instance a relocation in the city).

We propose here to study this question, and to examine to what extent city-wide actions can have an impact on urban heat island effect and heat wave vulnerability. We focus on a representative issue: whether compact or spread-out city developments can have a positive or negative impact on UHI and heat wave risk. The comparison between advantages and costs of compact and spread-out city developments has nourished a long-standing academic debate (see for example Newman and Kenworthy, 1989; Ewing, 1997; Gordon and Richardson, 1997; Ewing et al., 2003; Eid et al., 2008; Brueckner and Largey, 2008). This has been recently revived by climate issues and greenhouse gases emissions reduction concerns. A dense urban form indeed reduces urban expansion. It may help reducing urban travel distances and increasing public transport and non-motorized transport modal share, as well as reducing building energy use (see for instance OECD, 2012; Viguié and Hallegatte, 2012). However, city shape influence on UHI and, consequently, on heat wave vulnerability has been proposed as an important element of the debate. Higher densities may exacerbate UHI, in turn generating the need for more cooling and increasing energy use (McEvoy et al., 2006; Hamin and Gurran, 2009; Mees and Driessen, 2011). This is part of the "density conundrum" (Hamin and Gurran, 2009).

There is no clear consensus so far on how the city densification may influence UHI. Thus, the present study tries to shed new light on how different urban planning policies, leading to more or less compact city shapes, can impact the intensity and form of UHI. This impact is a priori not trivial to infer. The spread-out and compact city forms have different footprints, which may affect the spatial extent of UHI at city scale. In addition, the urban typologies favored by the different urbanization trends modify locally the types of land covers and the morphological characteristics. As an example, the spread-out city favours low-density urban typologies and the presence of vegetation, and limits the proportion of impervious covers, so that the UHI effect can be potentially mitigated. We study this question using Paris urban area as a case study, and compare the impact on UHI and heat wave vulnerability of different prospective city development scenarios.

This work is a result of a French research project (VURCA) that aimed at assessing the vulnerability and possible adaptation strategies of Paris metropolitan area to future heat waves. This issue has been investigated by accounting for the interactions of urban climate, local impacts of climate change, and the evolution of the city itself, thanks to an interdisciplinary approach involving researchers in climate, urban meteorology, economy, and buildings sciences and techniques.

The next section describes the numerical modelling methodology, more particularly the tools used for the production of urban expansion scenarios and the modelling of urban climate. Model evaluation is then presented in Section 3. Section 4 is dedicated to the presentation of indicators used to quantify and compare UHI effects. Finally, Sections 5 and 6 investigate how urban sprawl strategies impact the UHI and urban population. Section 7 concludes.

2. Modelling city evolution and urban climate

2.1. Overall methodology

The climate of Paris region – as it could be in 2100 under heat wave conditions – is studied by combining the local-scale effects of climate change on such extreme meteorological events and the impacts of urban sprawl. This analysis is carried out using a bottom-up approach. We use three steps simulations (see Fig. 1) in which both urban expansion scenarios and regional meteorological forcing conditions are used to feed a physically-based urban climate model.

We review in this section each of these three steps: maps of city evolution and sprawl scenarios are first created using a socio-economic land-use transport interaction model, NEDUM-2D, and technical assumptions about future buildings characteristics (Section 2.2, Step 1 in Fig. 1). Meteorological forcing is then built for an ensemble of heat-wave conditions varying in intensity and duration and defined starting from the analysis of regional climate projections (Section 2.3, Step 2 in Fig. 1). Finally, these two inputs are used by physically-based Town Energy Balance (TEB) urban canopy model in order to simulate the urban climate of Paris, especially the urban heat island (UHI), as well as the thermal comfort conditions for indoor and outdoor environments (Section 2.4, Step 3 in Fig. 1).

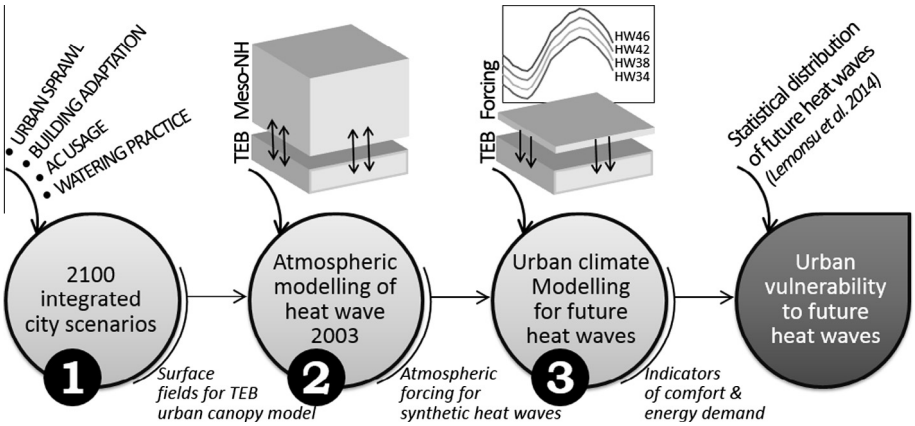

Fig. 1. Description of the interdisciplinary methodology implemented in the VURCA project.

2.2. City evolution scenarios

Paris urban area will evolve by the end of the century, as a result of macro-economic trends and demographic pressure, as well as under the influence of local urban planning policies, evolution of technologies and lifestyles. These combined effects can play a significant role on the structure of the city and, therefore, potentially, on the microclimate.

2.2.1. Urban expansion

To construct the urban expansion scenarios that we use here, long term socio-economic scenarios are downscaled at city scale using the method developed in Viguié et al. (2014). To do that, the land-use transport interaction model NEDUM-2D is used (see Appendix A). This model is based on a dynamic extension of the classical urban economic theory (Fujita, 1989), and explains the spatial distribution of land and real estate values, dwelling surfaces, population density and buildings heights and density across the city. It is here run for Paris area from 1900 to 2100. A validation over the 1900–2010 period shows that the model reproduces available data and captures the main determinants of city shape evolution over this period. A detailed description of the model and of its calibration can be found in Viguié et al. (2014).

In this study, a simple reference city expansion scenario is used, called the "spread-out city" scenario and referred to as *SPR* afterwards. It follows historical trends of Paris urban area evolution over the 20th century, but takes into account a sharp decrease in population growth, and in transport efficiency improvements – by assuming that transport speed will remain the same as today – over the 21st century (see Appendix A for more details). Fig. 2 shows a map of projected Paris urban area extension between 2010 and 2100 in this scenario. It is assumed in this case that the extension of the city is entirely guided by the market: we introduce no policy or regulation limiting the extension of the city or preferentially developing certain areas. The idea is that this scenario is used here to represent the "natural" trend of development of the city; this trend does not necessarily match the development that will occur in practice, but it allows understanding and anticipating land pressures, and therefore future local challenges.

Based on this scenario, we have then built four alternate city expansion scenarios, in which we make different assumptions about local land-use regulations (Figs. 3 and 4). In the "compact city" scenario (*COM*), strict urban containment policies are implemented in 2020, to control urban sprawl and protect natural areas and agriculture activity. From that year on, building is only possible through a densification of existing built spaces, but is prohibited elsewhere. In "green city" scenarios, no effective containment policy is carried out, but numerous parks are introduced in the city: in 2020, respectively 10% (*G10*), 30% (*G30*) or 50% (*G50*) of all built surfaces is uniformly destroyed to leave space for urban parks. After 2020, respectively 10%, 30% or 50% of all newly urbanized surfaces have to be urban parks (Fig. 3). These scenarios are of course somehow extreme, and unrealistic. They only aim to highlight what could be the impact of extreme theoretical greening scenarios.

As can be seen in Figs. 3 and 4, urban extension is larger in green city scenarios than in the spread-out city scenario, in which urban extension is itself larger than in the compact city scenario. Population is the same in each scenario, and built densities are consequently in the reverse order. Table 1 sums up main characteristics of the projected city development in 2100 in the five scenarios, and of the simulated urban area in 2008 (see also Appendix A). The urban area simulated by NEDUM-2D in 2008 is used in this study as a reference of the today city (*REF*). The state of the city for this date is exactly the same whatever the urban expansion scenario, since (as explained just above) the different hypotheses of urban planning applied in the scenarios only differ from 2020.

2.2.2. Buildings characteristics

Built-up areas in the simulated city can belong to one of four classes of urban typologies: Paris historic buildings ("Haussmannian architecture buildings"), collective housing, single housing, and office buildings. Except for Paris historical

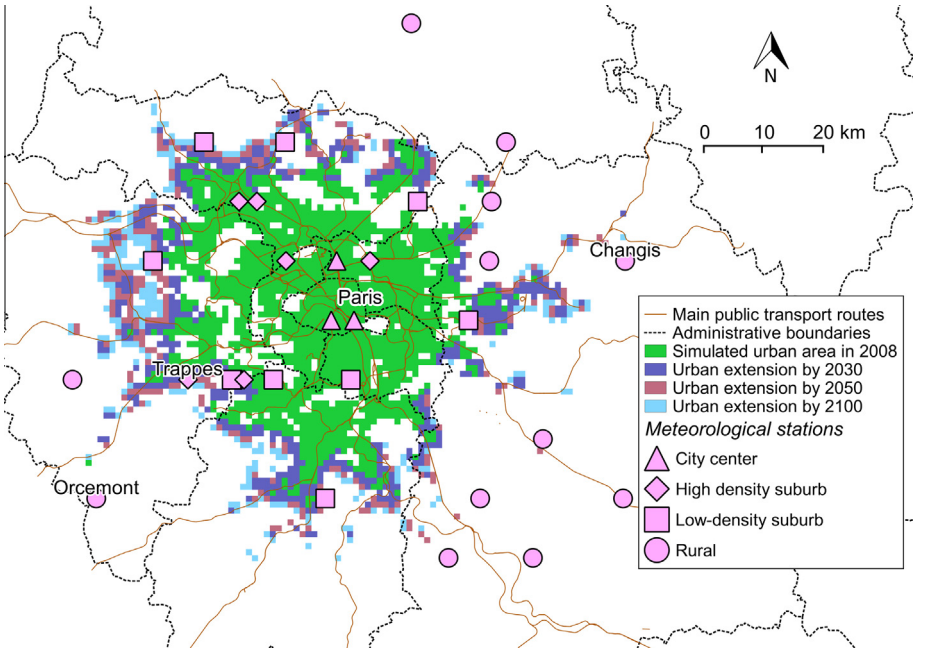

Fig. 2. Example of simulated urban area extension, in Spread-out city (*SPR*) scenario. Reference case (*REF*) corresponds to simulated urban area in 2008. Locations of the meteorological stations presented in Section 3.2 are also indicated.

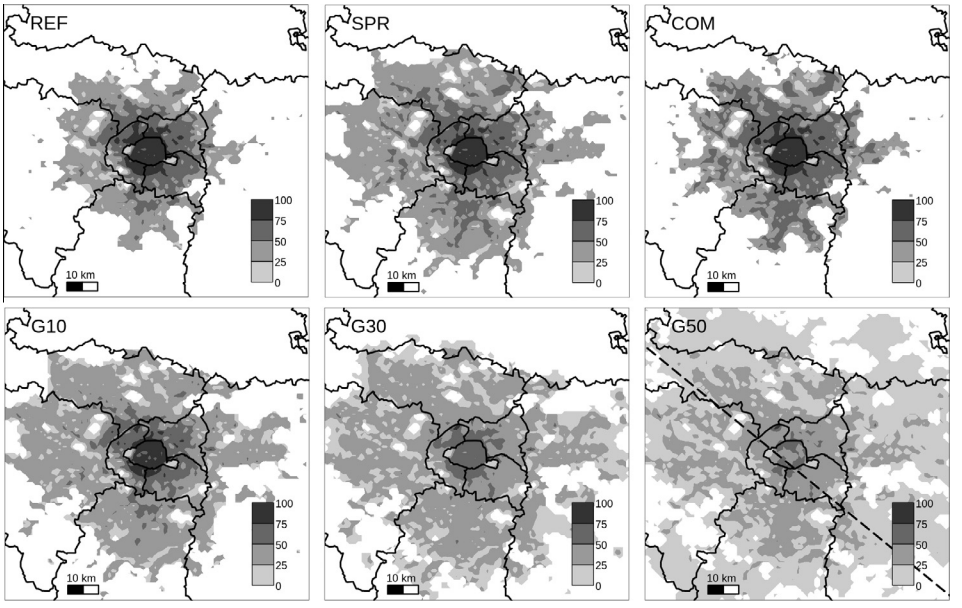

Fig. 3. Presentation of the *REF* case (in 2008) and the five urban sprawl scenarios, in 2100. The maps present the simulated percentage of impervious covers over the study area. The dotted black line in the last map shows the line along which the profile graphs are computed in Fig. 4.

buildings and office buildings, which are exogenously given (i.e. their locations, size and number are prescribed as input parameters and do not evolve with time), building type is endogenously determined as a function of the population density simulated by NEDUM-2D. This makes the surface devoted to collective housing and single housing slightly different in each scenario (see Appendix A). Each urban typology has its own characteristics in terms of roof types, insulation, etc. (see Appendix A for more details). Especially, collective housing is supposed to be better insulated than single housing. This hypothesis will be of importance when studying temperature inside the buildings (cf. Section 6.2).

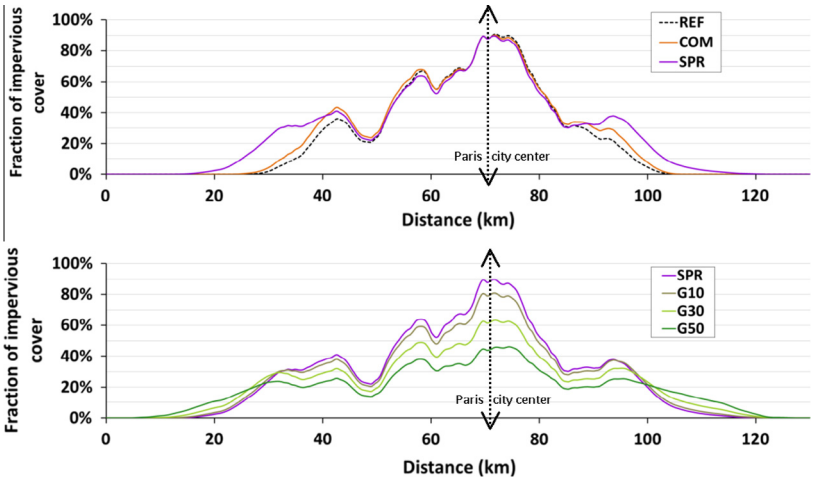

Fig. 4. Examples of impervious cover profiles over the study area.

Table 1
General characteristics of the reference city and of the urban sprawl scenarios simulated by the NEDUM-2D model. Note that the "urban mask" refers to the whole area that extends up to the boundaries of the city whereas the "city area" refers to the urban covers only (including urban green areas).

City	Description	Date	Urban pop (inhab.)	Urban mask (km^2)	City size (km^2)	Green areas (km^2)
REF	Today Paris	2008	11 000 000	2520	1910	820
SPR	Spread-out city	2100	12 500 000	4200	2240	910
COM	Compact city	2100	12 600 000	2960	3090	1420
G10	10% Green city	2100	12 700 000	4620	3410	1740
G30	30% Green city	2100	12 900 000	5710	4220	2600
G50	50% Green city	2100	13 200 000	7950	5750	4230

2.2.3. Air conditioning use and vegetation watering

In this study, we suppose as a simplification that no building is equipped by air-conditioning system. We also suppose that urban vegetation (but not forests neither agricultural fields) is watered during heat waves. Watering is done through a program of daily sprinkling, from 21 pm to 05 am with a sprinkling rate of $1.2 \cdot 10^{-7}$ m^3 s^{-1} of water (de Munck, 2013).

2.3. Heat-waves modelling

Lemonsu et al. (2014) showed from the analysis of a large set of regional climate model (RCM) projections that the Paris basin will be frequently affected at the end of the 21st century by heat waves which will be in average longer and more intense than today. Each of these heat waves is characterized by a maximum intensity, i.e. maximum temperature T_X reached during the event, and a duration in number of days. They have been classified according to four classes of intensities, i.e. with T_X between 32–36 °C, 36–40 °C, 40–44 °C, and greater than 44 °C. Starting from heat waves extracted from the RCM projections, the probabilities of heat-wave occurrence over Paris region for time period 2070–2099 have been computed for each class of intensities and all possible durations. This has been done by considering either the ensemble of events (Fig. 5, left) or the 10% most extreme events in a meteorological sense (i.e. by considering the product intensity × duration) (Fig. 5, right).

After this analysis of the characteristics of future heat waves at a regional scale, meteorological events are downscaled over Paris urban area. A set of idealized events varying in intensity and duration is built, based on the atmospheric modelling of a real meteorological event: the heat wave of year 2003. This is done for the four intensity classes with T_X of 34, 36, 38, 42 °C previously identified from the climate projections. These classes of heat waves are afterwards referred to as *HW34*, *HW38*, *HW42*, and *HW46*. For each of them, the durations can vary from three to 38 days. The complete methodology of idealized heat-wave building is detailed in Appendix B, and the evaluation of the modelling exercise by comparison with meteorological observations is presented in Section 3.

2.4. Urban climate modelling

The urban climate is simulated by using the physically-based TEB urban canopy model (Masson, 2000; Hamdi and Masson, 2008). It parameterizes the energy, water, and momentum exchanges between urban covers and atmosphere, so that it is able to simulate the urban climate from the neighbourhood to the city scale by distinguishing various typologies of urban blocks thanks to different sets of geometrical parameters and material properties. Recently, TEB has been improved

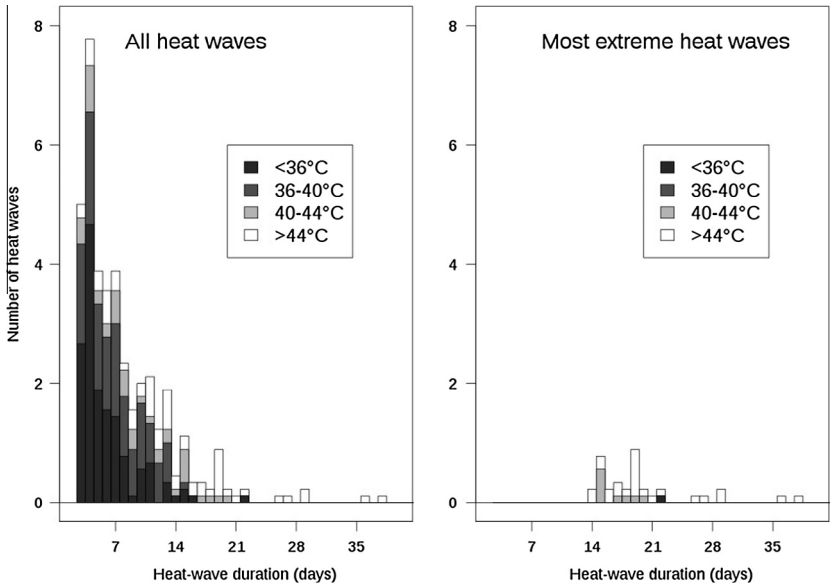

Fig. 5. Statistical distribution of heat waves for 2070–2099 time period according to the four classes of intensity, and by considering all events (left) or the most extreme ones (right). These events have been extracted by Lemonsu et al. (2014) from regional climate model projections provided by the ENSEMBLES project.

in order to include a building energy module (Bueno et al., 2012; Pigeon et al., 2014) and to simulate the evolution of air temperature inside buildings. By accounting for local interactions between built-up covers and urban green areas (Lemonsu et al., 2012), TEB coupled to the ISBA vegetation model (Noilhan and Planton, 1989) is also able to model the potential cooling effect of vegetation in urban environment linked to evapotranspiration process of plants.

The TEB model is run in offline mode to simulate the climate of Paris over a domain of 100 km × 100 km with a horizontal resolution of 1 km (see the domain in Fig. 2). It is forced by the atmospheric forcing coming from the idealized heat waves *HW34*, *HW38*, *HW42*, *and HW46*. As output, TEB provides the near-surface meteorological fields (e.g., temperature, humidity, wind speed at street levels) with a one-hour time step. Besides standard variables, TEB also computes the Universal Thermal Climate Index (UTCI, Fiala et al., 2012) – result of the European Cooperation in Scientific and Technical Research (COST Action 730, http://www.utci.org). This represents the "perceived" temperature of the people, and it takes into account four immediate meteorological condition variables: air temperature, humidity, wind, and radiation. This UTCI is computed both for indoor and outdoor environments.

3. Models evaluation

3.1. Methodology

Model evaluation is an important aspect of prospective studies. Both NEDUM-2D model (see Viguié and Hallegatte, 2012; Viguié et al., 2014) and TEB urban canopy model (see Masson et al., 2002; Lemonsu et al., 2004; Pigeon et al., 2008) have already been separately validated against empirical or experimental data. However these models do, of course, not exactly describe the reality, and errors from each model can propagate through the modelling chain. We therefore evaluate here the ability of the chain, i.e. TEB urban canopy model using as input the urban area simulated by NEDUM-2D, to simulate the urban climate of Paris.

It is not rigorously possible to prove that, using our methodology, the impacts of different scenarios of urban expansion on urban climate can be correctly simulated and quantified. What we can do, however, is to check whether our modelling chain is at least able to adequately model past heat waves. The evaluation exercise is done for the 10th of August 2003, taken here as reference day of the 2003 heat wave. This is the day which is used in this study to build the idealized heat waves (see Section 2.3).

This event has been simulated with the Meso-NH atmospheric model (Lafore et al., 1998) coupled to the SURFEX surface module (Masson et al., 2013b) including TEB (see Appendix B for details). TEB is initialized by the map of Paris urban area that NEDUM-2D simulates for the year 2008 (the simulated city is almost unchanged between 2003 and 2008). The starting point for this NEDUM-2D simulation is 1900, and the map used is the map obtained when simulating 108 years of city evolution after 1900. This map does share mainly similarities with actual Paris urban areas characteristics in 2008, but it is of course not exactly similar, due to NEDUM-2D approximations.

We have then compared with observed data, at the neighbourhood scale, resulting simulated urban climate of Paris for the 2003 heat wave, as well as its spatial variability. This simulation, which we call *REF*, will be used several times in the rest of this study as a benchmark for the assessment of the impacts on urban climate of the different urban planning scenarios.

3.2. Comparison to meteorological observations

Over the study area, 31 meteorological stations from the Météo-France operational network are available and provide the 2-m air temperature and humidity, as well as the 10-m wind speed and direction with a 1-h time step (see Fig. 2 for the locations of stations).

The records of each station can be compared to the model's outputs extracted at the grid point the closest to the station geographic location. However, a point-by-point comparison between modelled and observed data is not appropriate to the 1-km horizontal resolution of the model that can result in significant subgrid heterogeneity of surface characteristics. For this reason, the comparison is performed by gathering the stations (i.e. averaging their data) regarding to the building density in the corresponding model's grid point and the distance to the city core. Four zones are distinguished and presented in Fig. 2: (1) Paris historic city centre (3 stations), (2) high-density suburbs (6 stations), (3) low-density suburbs (10 stations), and (4) rural areas (12 stations), with respective building densities of 50–60%, 10–25%, 2–10%, and 0%.

The daily evolution of the average temperature and the associated spatial variability (as error bars) of each zone for both observations and model's outputs are presented in Fig. 6. In addition, the statistical scores are computed over the nighttime (2200-0500 UTC) and daytime (0600-2100 UTC) periods and presented in Table 2. Based on the averaged values, the best results are obtained in the city centre with biases and root mean square errors (RMSE) always lower than 1 °C. They slightly deteriorate for high- and low-density suburbs but are still acceptable (1.5 and 2.1 °C at maximum, respectively for biases and RMSE). Slight underestimation of temperature during daytime and slight overestimation at night are systematically observed in model outputs. This effect is more marked in the countryside where the model simulates air temperatures which are too high when compared to observations due to a defect in the calculation of vertical exchanges in low atmosphere for stable conditions.

It is important to notice that whatever the zone, the second simulated night is always closer to the observations than the first one. This systematic underestimation in nocturnal temperature (quite important in the most vegetated areas) between the 9th and 10th of August 2003 was already highlighted by the previous numerical studies CLIM2 (de Munck et al., 2013) and EPICEA (Kounkou-Arnaud et al., 2013). It might be due to the synoptic or regional-scale wind calculation that drives the horizontal advection or in soil water content conditions that initiates the surface exchanges. In the study area, however, no

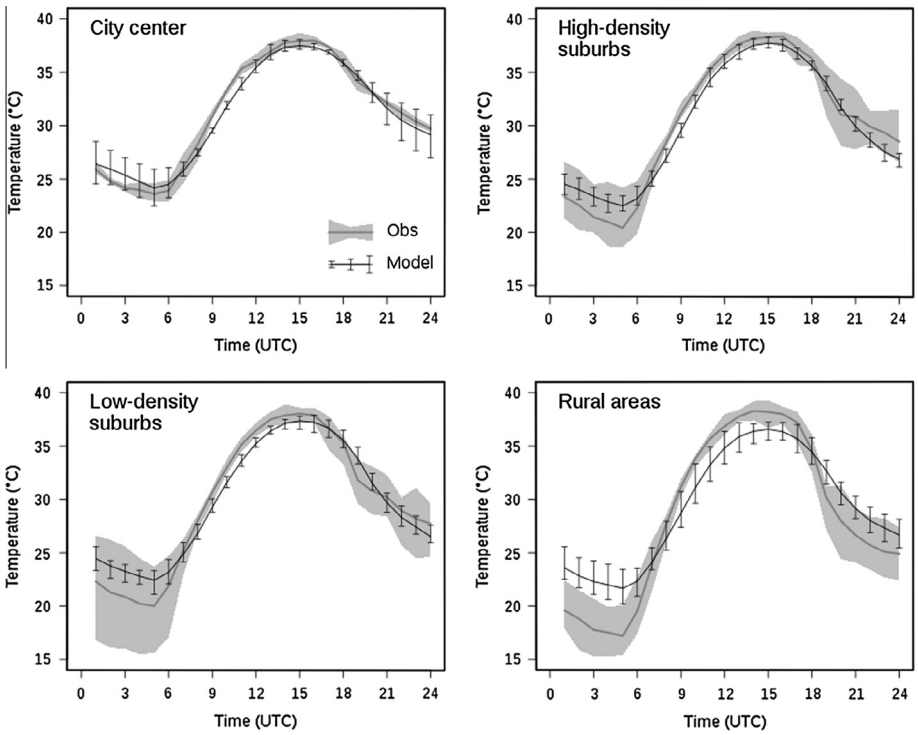

Fig. 6. Comparison between observed and modelled 2-m air temperatures on the 10 August 2003 averaged for the four land cover classes. The standard deviations are also presented both for model outputs (black bars) and observations (grey envelop).

Table 2
Biases (Obs-Model) and root-mean square errors computed between observations and model outputs for the four land cover classes and separately for nighttime (2200-0500 UTC) and daytime (0600-2100 UTC) hours.

		City centre	High-density suburbs	Low-density suburbs	Rural areas
Bias (°C)	Night	−0.41	−0.79	−1.51	−3.72
	Day	+0.50	+0.62	+0.41	+0.57
RMSE (°C)	Night	0.83	1.69	2.07	3.83
	Day	0.78	0.94	1.08	2.06

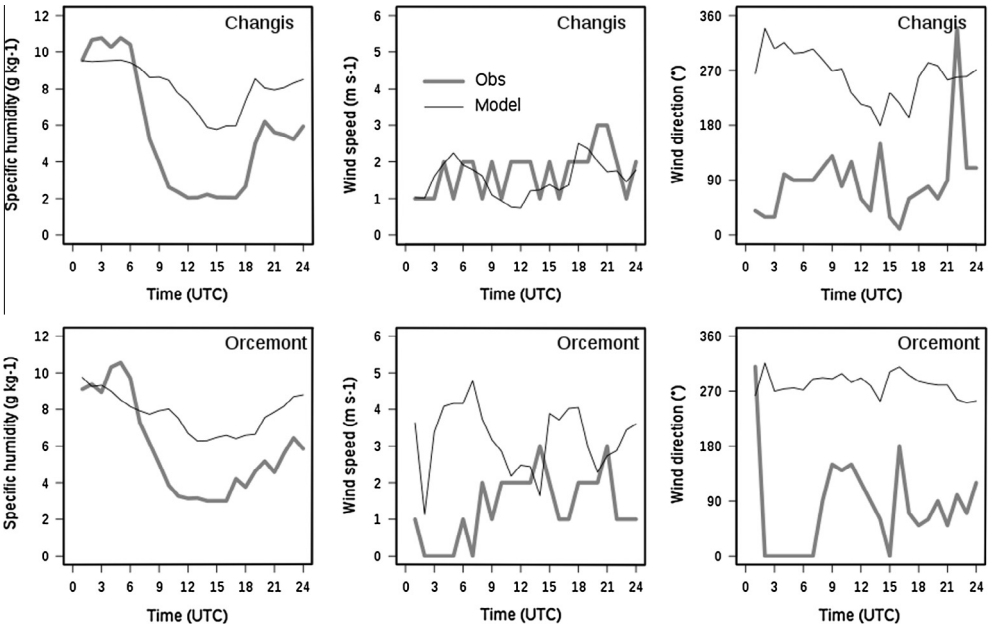

Fig. 7. Comparison between observed and modelled 2-m specific humidity, and 10-m wind speed and direction on the 10 August 2003 for the two rural stations of Changis (top) and Orcemont (bottom) located north-east and south-west of Paris, respectively.

record is available for soil water content and too much data are missing in the radio soundings daily launched at Trappes (South of Paris, see Fig. 2) in order to provide relevant information that could highlight model defects.

Failing this, observed and modelled data of wind speed and direction, as well as water vapour mixing ratio, are compared for the two rural stations of Changis and Orcemont located respectively North-East and South-West of the city (see Fig. 2 for locations). Even if the wind speed measures recorded at the South-West station are lower than the model calculations, intensities keep the same magnitude order for both stations. Also, taking into account the weakness of the wind speed, both intensity and direction (Fig. 7) stick to the stations data even though the model does not get all the variability due to the instantaneous measures. The same behaviour appears whatever the station considered, either in the city centre or the suburbs (not shown here). For humidity, the main difference is observed during the day (Fig. 7) where air humidity is significantly higher in the model (+4 g kg^{-1}). This is coherent with the underestimation of air temperature at the same time, since the near-surface conditions are strongly driven by the soil state and the partition between latent and sensible heat fluxes in the surface energy balance. Nonetheless, the systematic overestimation of the temperature during the night is not explained by these results.

Despite a misrepresentation of rural areas temperature (especially at night), the coupling between NEDUM-2D, SURFEX, and MesoNH therefore leads to a quite satisfying modelling of the Parisian urban climate in the conditions of the 2003 heat wave. The system appears able to reproduce the spatial variations in air temperature observed between the various urban landscapes.

4. Quantification of UHI effect

Different solutions exist to measure or more broadly to quantify UHI, either from observations or from modelling (Schwarz et al., 2011). In literature, the UHI is often defined as the difference in temperature between the city centre and a reference point in the surrounding countryside, i.e. it informs the maximum effect reached at city-scale but does not provide spatialized information on all areas potentially affected. We use here this indicator, but we also propose a more

innovative approach, and measure also UHI importance – both at nighttime and daytime – based on other indicators of UHI and thermal stress (these indicators are all listed in Table 3). They enable to objectively assess the vulnerability of the city to heat waves, and to compare the various urban sprawl strategies (see Step 4 in Fig. 1).

4.1. Definition of indicators

- Temperature anomaly
  This is the standard difference in temperature between the city centre and a reference point in the surrounding countryside. By using the simulations of the various heat waves varying in intensity and duration, a relative nighttime or daytime temperature anomaly is calculated at a daily basis for each scenario at each grid point i as:

$$\Delta T_{sc}^{night}(i) = T_{sc}^{night}(i) - T_{rur}^{night}$$

$$\Delta T_{sc}^{day}(i) = T_{sc}^{day}(i) - T_{rur}^{day}$$

  T_{rur}^{night} and T_{rur}^{day} are the nighttime and daytime reference temperatures, respectively, of the rural environment. They are computed from the *REF* scenario by a spatial averaging of the nighttime and daytime temperatures, respectively, modelled at the non-urbanized grid points located at the boundaries of the domain.
- City fraction indicator
  By considering several threshold values (from +0.5 to 2.5 °C) which reflect the severity of the UHI, the city's area affected by UHI (referred to as A_{UHI} in km^2) can be computed. Since the spatial extent of the city varies with the urban expansion scenario, the fraction of the city affected by UHIs (referred to as F_{UHI}) is also computed by normalizing A_{UHI} by the city size. This indicator can be related to indicators of surface UHI (Streutker, 2003; Xu et al., 2004) computed from satellite land surface temperature measurements (Schwarz et al., 2011).

- Population fraction indicator

  To complete previous indicators, an indicator related to the affected population (referred to as P_{UHI} in %) is defined as the proportion of the city inhabitants affected by the different thresholds of UHI. In this study, this can be done because NEDUM-2D model provides simulations of the spatial distribution of urban population over the study area.

- Heat stress duration indicators

  Two additional indicators are computed to assess potential health impacts of UHI. They are based on the UTCI computed by TEB inside buildings and in the streets. This UTCI can be associated to a scale of heat-stress levels, for extreme cold and especially for extreme heat (Bröde et al., 2012). The heat-stress indicators are calculated here as the number of hours per day that is spent in a level of strong heat stress (i.e. for UTCI > 32 °C) both for indoor conditions (referred to as SHS_{in}) and shaded outdoor conditions (referred to as SHS_{out}).

4.2. Application to the reference case

Let us illustrate these indicators in the reference scenario (*REF*). The maps of the various thresholds of UHI – both for night and day – obtained for this scenario after seven days of *HW38* are presented in Fig. 8 (globally, similar patterns are noted for the other scenarios, and are not shown in this paper). Note that this idealized heat wave is rather close to the real conditions of the 2003 heat wave in Paris region that lasted about 8 days with slightly variable daily conditions.

Table 3
Description of indicators used for assessing urban sprawl strategies. The two last columns compile the values of the indicators calculated for *REF* in the case of a seven-day *HW38*. As an example, A_{UHI}, F_{UHI}, and P_{UHI} are here computed for a temperature threshold of 1.5 °C.

Indicator (Unit)		Definition	*REF* (night)	*REF* (day)
ΔT	(°C)	UHI computed as a temperature difference between a given location and a reference rural environment	2.84	0.57
A_{UHI}	(km^2)	Area of the city affected by UHI, for a given threshold of ΔT	217	192
F_{UHI}	(%)	Fraction of the city affected by UHI, for a given threshold of ΔT	12	11
P_{UHI}	(%)	Fraction of population affected by UHI, for a given threshold of ΔT	42	6
SHS_{out}	(hrs day^{-1})	Number of hours spent per day in strong heat stress conditions in outdoor shaded environment, averaged over the population	12.52	
SHS_{in}	(hrs day^{-1})	Number of hours spent per day in strong heat stress conditions inside buildings, averaged over the population	9.15	

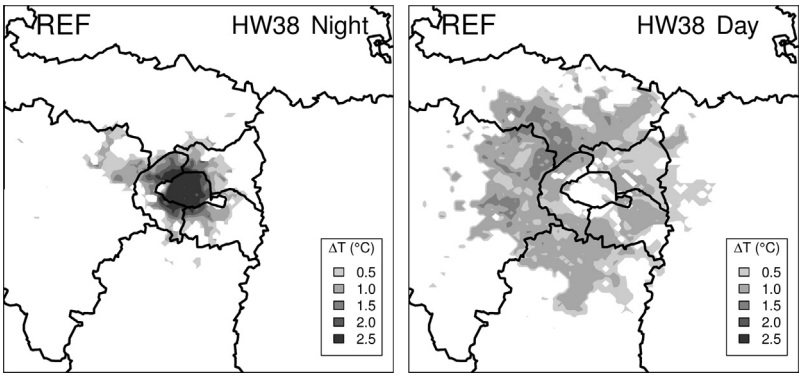

Fig. 8. Spatial representation of the city's areas affected by UHI for the different thresholds in temperature anomaly. Example of the today city (*REF* scenario) for the *HW38* after seven days of heat wave both for nighttime (left) and daytime (right) hours.

The UHI systematically spreads more during the day than at night, and presents different patterns. As expected, the nocturnal UHI is concentrated over the city centre and the densely built-up suburbs but rapidly decreases and becomes insignificant (i.e. less than 0.5 °C) beyond 5 km from the city core. This organization is driven by the process of heat release from urban infrastructures that occurs at night and that is mostly observed in dense urban areas. Inversely during the day, the city centre is less affected by UHI, because it is partially protected from incident radiation due to shading effects related to the high building density. Such effects have already been highlighted by Oke (1982) and Steeneveld et al. (2011). Besides, as shown in Lemonsu et al. (2012), the residential districts undergo cumulative effects of urban warming and soil drying under heat wave conditions. Table 3 summarizes indicator value in this *REF* case both for nighttime and daytime hours.

At night, the maximum UHI reaches 2.84 °C for the city centre compared to the surrounding countryside. The proportion of the city affected by UHI is not very important: F_{UHI} = 12% if a 1.5 °C threshold is used for ΔT. Nonetheless, this area concentrates urban population; this leads to a great proportion of inhabitants affected by UHI (P_{UHI} = 42% in this case). During daytime, whereas F_{UHI} = 11%, i.e. the same proportion of city than at night, the proportion of inhabitants affected by UHI is much lower (P_{UHI} = 6%) since the positive anomalies of temperatures are essentially observed over low-density urban areas. Note that we consider here the fraction of inhabitants as defined by their place of residence: we do not model in our simulations the fact that people can be outside their home (e.g., at work) during the day. So this fraction is actually a measure of the percentage of residences affected by the temperature.

The heat stress level evolves with time according to the hour of the day but also day after day during the heat wave. This evolution is presented in Fig. 9 for indoor and outdoor environments after three, seven, and 14 days of heat waves. Inside buildings, the level of thermal comfort is rather stable during the day. This is due to thermal insulation and inertia of constructions. However, the thermal comfort deteriorates day after day for long-lasting heat waves, as the buildings get warmer progressively. As an example, it is found that after seven days of *HW38*, people spend in average about nine hours per day in strong heat stress conditions with UTCI values varying between 32 and 33 °C (according to Table 3).

In the streets, the UTCI evolved during the day mainly in response to solar radiation. Day after day, its daily profile remains broadly unchanged whatever the heat-wave duration. Consequently, for outdoor conditions, the number of hours

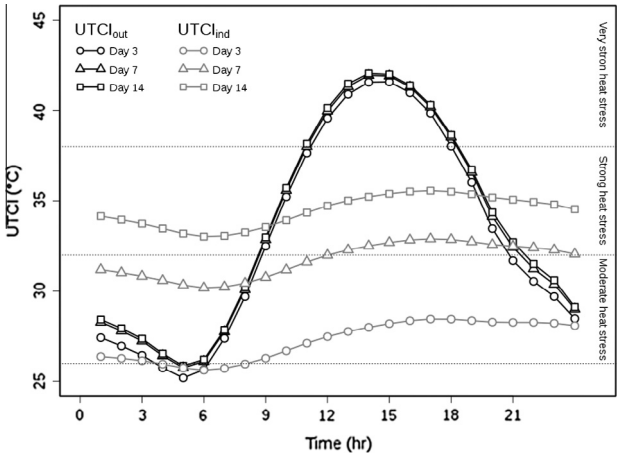

Fig. 9. Daily evolution of indoor and outdoor UTCI for *HW38* after three, seven, and 14 days of heat waves, respectively. Indoor and outdoor UTCI are computed for each grid point of the domain and spatially aggregated at the city scale.

of discomfort, accumulated over the event duration and expressed as a daily average, is approximately the same. After seven days of *HW38*, people spend in average 12 h and 30 min per day in strong heat stress conditions in the streets. On average, this result is comparable to what is obtained for indoor conditions but the heat stress is much higher outside than inside buildings in the middle of the day since the UTCI rises up to 42 °C (see Fig. 9). Inversely, outdoor conditions are more comfortable than indoor conditions during night because the nocturnal cooling is more marked.

5. Impact of urban sprawl scenarios on UHI: Amplitude and extension

UHI is affected by city expansion scenarios. We examine here how this is reflected by our indicators.

5.1. UHI amplitude for Paris city centre

The city centre of Paris is an area of specific interest because the highest values of UHI are observed there. Fig. 10 shows a comparison of UHI temperature anomaly (indicator ΔT) for the city-centre grid points, i.e. for which the urban typology is defined as Paris historic buildings (see urban typology map in Fig. A3 of Appendix A). Let us first compare scenario *SPR* and the green city scenarios *G10*, *G30* and *G50*. Night UHI intensity is equal to 2.78 °C for *SPR* and appears to decrease with the implementation of greening strategies. Contrary to what could be expected, the development of new neighbourhoods which encroach on natural areas tends to limit the UHI. This effect is due to the low building density of these neighbourhoods and to the fact that gardens are supposed to be watered in the present study (Section 2.2.3). The UHI mitigation is also perceptible over the city centre where additional urban green areas are set-up. This mitigation reaches 0.19, 0.66, and 1.08 °C for *G10*, *G30*, and *G50*, respectively, compared to *SPR*.

The contrary, however, occurs during the day: the UHI magnitude in the city centre is reinforced for the greenest scenarios (Fig. 10) of +0.12, +0.24, and +0.61 °C for *G10*, *G30*, and *G50*, respectively. This is due to the fact that the greening policies we consider here decrease urban compactness and lead to larger sky-view factors and a greater sun light exposure. Nonetheless, these UHI intensities are weaker than those reached at night whatever the scenario, and do not exceed 1.5 °C.

Comparing scenarios *SPR* and *COM*, i.e. analysing the impact of city densification, leads to a different result. Both at night and during the day, the temperature anomaly appears slightly higher in *SPR* scenario than in *COM* scenario (2.78 against 2.67 °C, and 0.90 against 0.69 °C, for night and day, respectively). These differences are small, however, and not strongly significant (lower than 0.2 °C) because for these two scenarios, the morphology of the historic city centre remains unchanged, i.e. the local characteristics of the city at the point where the temperature anomaly is measured is the same in these scenarios. Consequently, using temperature anomaly indicator, it is tricky to conclude on the impact of city density on UHI.

Finally, the *REF* case gives the lowest intensity of UHI during the day, but the highest one at night. For the "today city", building characteristics are slightly different than for city evolution scenarios, because the scenarios assume a progressive improvement of thermal regulation with time (see Appendix A). More especially, in the future some of buildings are equipped with reflective materials. As a result, they store less energy during the day and release less heat at night, which can explain that the nighttime UHI is the highest for *REF*. Inversely, the fact that the city's size is smaller for *REF* than for all scenarios could explain the lowest value of daytime UHI.

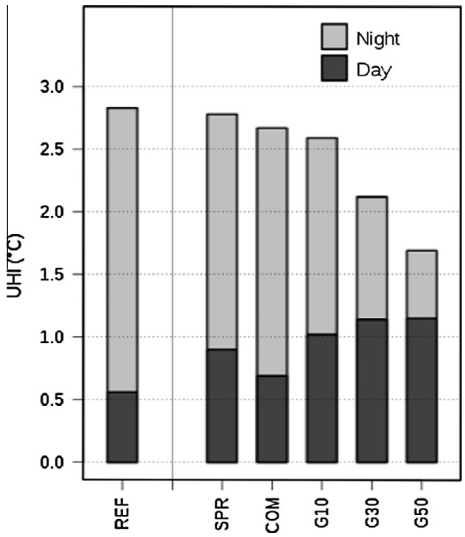

Fig. 10. Comparison of the values of UHI obtained by aggregating the results for the city-centre grid points for each scenario for the *HW38* after seven days of heat wave.

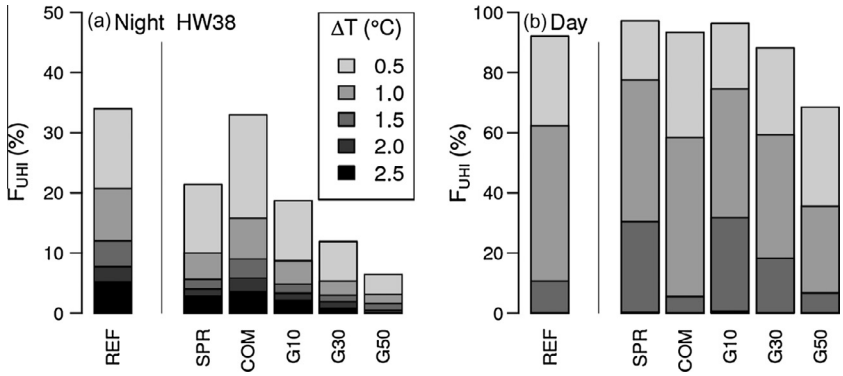

Fig. 11. Comparison of the proportion of the city affected by UHI according to the thresholds in temperature anomaly, for the today city and the future scenarios. Example of the *HW38* after seven days of heat wave both for nighttime (left) and daytime (right) hours.

Using UHI temperature anomaly as an indicator leads therefore to somehow inconclusive results. On the one hand, the effect of city densification cannot be significantly measured, and on the other hand the impact of the vegetation appears unclear, as it reduces UHI during the night but increases it during the day. Using alternative indicators can enable to get a clearer view of the differences between each scenario.

5.2. Fraction of city affected UHI at nighttime

Fig. 11 shows city fractions affected by UHI (indicator F_{UHI} of Section 4.1) at nighttime, for different temperature thresholds, in the case of *HW38* after seven days of heat wave. For each threshold, the same trend can be seen between scenarios: the denser the city, the most it is proportionately affected. *COM* is the most affected city, then *SPR*, *G10*, *G30*, and *G50*, whereas, conversely, these scenarios are more and more extended spatially. Contrary to the temperature anomaly indicator, F_{UHI} shows a non-negligible impact of city densification (i.e. a significant difference between *COM* and *SPR*).

The main reason behind these results is that the new urban areas that develop around the existing city are mainly low-density residential districts (where vegetation is widely present) that are consequently minimally affected by the nocturnal UHI. Therefore, the more spread-out the city, the lower the fraction affected by different UHI thresholds. Similarly, in all scenarios, projected cities in 2100 appear less affected by UHI than present day city, even without specific adaptation.

Both duration and intensity of heat waves have an impact on UHI because heat storage in soil and urban infrastructures, as well as soil water status, evolve during the event. By selecting the UHI threshold of 1.5 °C, the F_{UHI} indicator is computed day by day (from three days to three weeks) for the *REF* case and the five urban sprawl scenarios according to the four intensity classes (Fig. 12).

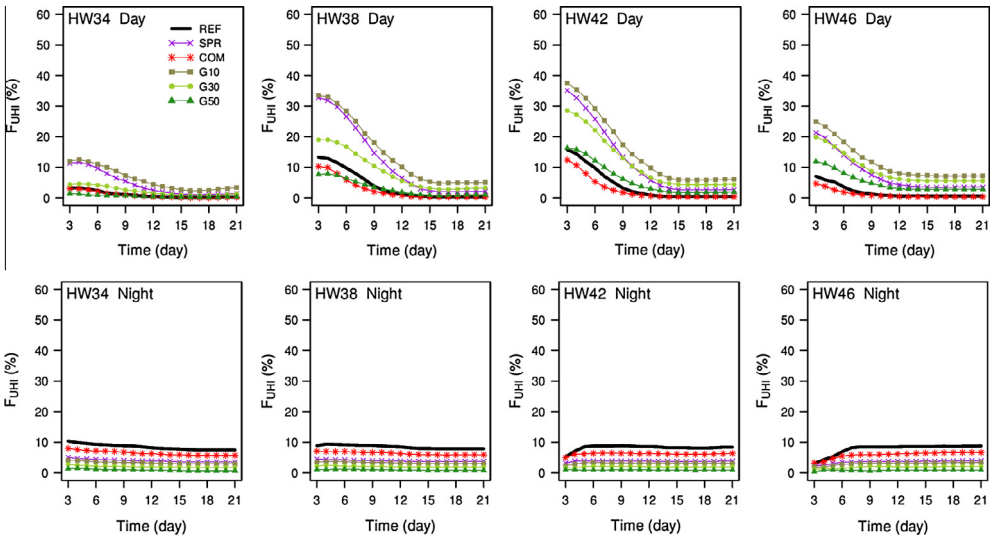

Fig. 12. Comparison of the evolution with time (from three to 21 days) of the proportion of the city affected by a UHI of 1.5 °C for the today city and the future scenarios. The results are presented for the four classes of heat-wave intensity, and both for daytime (top) and nighttime (bottom) hours.

The fact that the city is proportionally less affected at night when it is wider is confirmed whatever the intensity and duration of heat waves. The values of F_{UHI} reach rapidly an equilibrium value after few days of heat wave. Beyond the first week, F_{UHI} varies only slightly and is very similar whatever the intensity of heat waves. Indeed, for long events, the potential of heat storage decreases as the buildings warm up and the UHI does not evolve anymore. As an example, for the most unfavourable case *HW46*, the fraction of the city affected by UHI is about 12% for *REF*, 9% for *COM*, 5% for *SPR*, 5% for *G10*, and only 3% for *G30* and 1% for *G50*.

In conclusion, among the tested urban planning scenarios, the compact city appears the most affected to nighttime UHI. Inversely, the scenarios with vegetation reduce UHI spatial extension due to combined effects: the loose urban fabric reduces heat storage in urban infrastructures and watered green areas cool the ambient air through plants transpiration and evaporation of water intercepted on the foliage.

5.3. Fraction of city affected by UHI at daytime

At daytime, the conclusions are different (Fig. 12). For *HW34*, for instance, *COM* is the least affected by UHI, i.e. F_{UHI} is the lowest, and almost equal to F_{UHI} in the *REF* case. Inversely, the *SPR* scenario is the most affected city. The green city scenarios give intermediate results with a positive effect (i.e. mitigation of UHI) of a greening rate increase from *G10* to *G50*.

Let us look into the details at Fig. 12. Scenarios *COM*, *SPR* and *G10* are a bit more affected by UHI when the intensity of heat waves increases, but F_{UHI} mainly increases for *G30* and *G50* up to proportions which become very close to those of *SPR* and *G10*. In all scenarios, the values of F_{UHI} strongly decrease during the first two weeks of heat wave, and then stabilize.

The dynamics of UHI (and of the city's fraction affected) according to the intensity and duration of heat waves is driven by the availability of water for vegetation both inside (urban parks) and outside (forests and crops) the city. For short events, the high evapotranspiration of the surrounding vegetation has a more efficient cooling effect than that of urban green areas, which reinforces the UHI effect. For the longer events, the natural soils become drier while the urban green areas are still watered, so that F_{UHI} decreases. But after around two weeks of heat wave (depending on the intensity), this decrease in F_{UHI} stops because the water supply for urban vegetation is no more sufficient. This effect is especially marked for the most intense heat waves (see *HW46* in Fig. 12); the green scenarios become therefore significantly less effective.

In conclusion, the compact city *COM* clearly stands out from other urban expansion scenarios, more especially for long and/or intense events; by limiting the penetration of incoming solar radiation due to its dense urban form, it is the most efficient in mitigating UHI during daytime, regardless the intensity of heat wave.

Compared to the temperature anomaly indicator, nighttime and daytime F_{UHI} enable therefore to get a different view of the impact of the different scenarios. The ΔT indicator gives non-significant results for the impact of densification, and inconclusive results about the impact of the vegetation. In this case indeed, a positive effect (i.e., a temperature decrease) is obtained at night, but the effect becomes negative during the day with an increase in temperature. However, F_{UHI} highlights a different message: vegetation appears positive both for night and day, and densification now appears negative at night and positive during the day.

6. Impact of urban sprawl scenarios on UHI: Link with population distribution

As we have shown in the last section, the analysis of the impact of urban form on UHI depends on the indicator which is used. The indicators that we have used so far (ΔT and F_{UHI}) are related to the geometry of the urban micro-climate. In this section, we introduce in the analysis the spatial repartition of the population, and use the three last indicators of Table 3.

6.1. Fraction of population affected by UHI

Let us first translate the proportion of the city affected by UHI (F_{UHI}) into the proportion of population that is affected by UHI (P_{UHI}). To do that, we need to know the spatial distribution of the inhabitants, today and in the future. This can be done here thanks to the NEDUM-2D model that simulates the households' settlement dynamics (see Viguié et al., 2014).

The trends for the various heat waves are presented in Fig. 13. They are similar to those obtained for F_{UHI} but the orders of magnitude are very different. Especially, whereas, with F_{UHI}, the orders of magnitude of daytime and nighttime fractions are similar, this is no longer the case with P_{UHI}. Comparing scenarios on day 21 in Fig. 13, nighttime fractions vary between 0% and 10%, whereas daytime fractions vary between 10% and 40%. Same comparison in Fig. 12 shows variations between 0% and 10% both in daytime and nighttime.

At night, the benefits brought by the greening scenarios, which seem rather limited when evaluated according to the city surface proportion, are much more significant when evaluated according to the city population proportion. The *G50* green scenario, which is the most effective for mitigating the nocturnal UHI, leads to a reduction of more than 20% of the population affected by UHI (for a threshold of 1.5 °C as shown in Fig. 13) compared to the compact city *COM*, because the effects are mostly perceived in the most populated areas.

As for F_{UHI} indicator, *COM* appears the best choice for limiting UHI in daytime, but the worst in nighttime. However, introducing in the analysis the repartition of the population in the city, i.e. using P_{UHI}, has given new information: it shows that daytime effect of scenario choice has, to some extent, a much lower magnitude than nighttime effect. Therefore, when

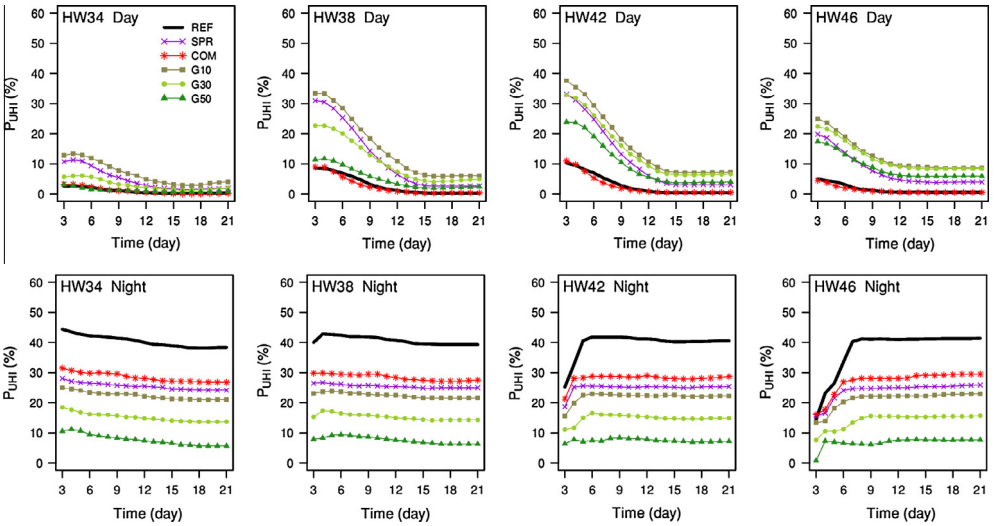

Fig. 13. Comparison of the evolution with time of the proportion of the population affected by a UHI of 1.5 °C for the today city and the future scenarios. The results are presented for the four classes of heat-wave intensity, and both for daytime (top) and nighttime (bottom) hours.

considering P_{UHI} indicator, the dense scenario seems in overall less desirable than spread-out city scenario. To go further, one needs indicators which integrate both nighttime and daytime effects. This is what is doing our last indicators SHS_{in} and SHS_{out} (Table 3).

6.2. Averaged thermal comfort

The last analysis framework that we consider in this study is the number of hours per day, on average for the whole heat-wave duration that is spent in strong heat stress conditions. For each city scenario and each simulated heat wave (for the four intensity classes and all possible durations), this indicator is computed both for indoor and outdoor conditions (SHS_{in} and SHS_{out} indicators are more detailed in Section 4.1 and Table 3).

These indicators are spatially aggregated by accounting for the spatial distribution of population density, in order to attribute greater importance to the most populated areas. They are then weighted by the occurrence probabilities of the future heat waves. We also compute, for extra information, the average for only the 10% most extreme heat waves (see Section 2.3 and Fig. 5 for detail).

6.2.1. Outdoor thermal comfort

For *REF* case (i.e. today city), we simulate that about 35%, 50%, and 15% of inhabitants spend, respectively, 16, 14, and 12 h per day in strong heat stress conditions (Fig. 14): heat waves can have an important effect on thermal comfort. The comparison of this *REF* case to the city scenarios in 2100 indicates that whatever the scenario, the outdoor thermal comfort is improved for a part of the population.

Particularly, the implementation of large-scale greening policies seems quite efficient. For the highest greening rate, less than 10% of inhabitants spend 16 h per day in SHS_{out} (against about 30% for instance in the business-as-usual *SPR* scenario). The improvements brought by the green scenarios mainly concern the residential areas, considering that the lower the building density is, the less heat storage there is. In addition, as shown by the statistical distribution of future heat waves (Fig. 5), a large proportion of these events has a characteristic temperature T_X lower than 40 °C and a duration lower than two weeks. As a result, the water supply prescribed for green areas is enough to produce a significant cooling which still reduces the daytime heat storage in residential areas. In the densely built-up districts, the proportion of green areas is lower and consequently, the cooling effect induced by evapotranspiration is more limited. On the contrary, the compact city *COM* is the most unfavorable scenario: as was suggested by P_{UHI} comparisons, nighttime increased UHI more than counterbalance daytime UHI decrease.

The comparison of SHS_{out} for the most extreme events (Fig. 14) leads to the same conclusions between scenarios. It can be however noted that for such heat waves, the heat stress conditions reach exceptional levels even for the most efficient urban planning scenarios: the entire city undergoes at least 18 h of SHS_{out} per day and 20% and more of population (according to the scenario) spends more than 22 h per day in SHS_{out}. In this case, alternative actions should be implemented in order to preserve the population-at-risk and to avoid serious sanitary consequences.

6.2.2. Indoor thermal comfort

With regard to indoor thermal comfort, the most unfavourable conditions also concern the city centre where people spend between 12 and 14 h a day in SHS_{in} (Fig. 14). This is related both to the UHI and to the bad energetic performances

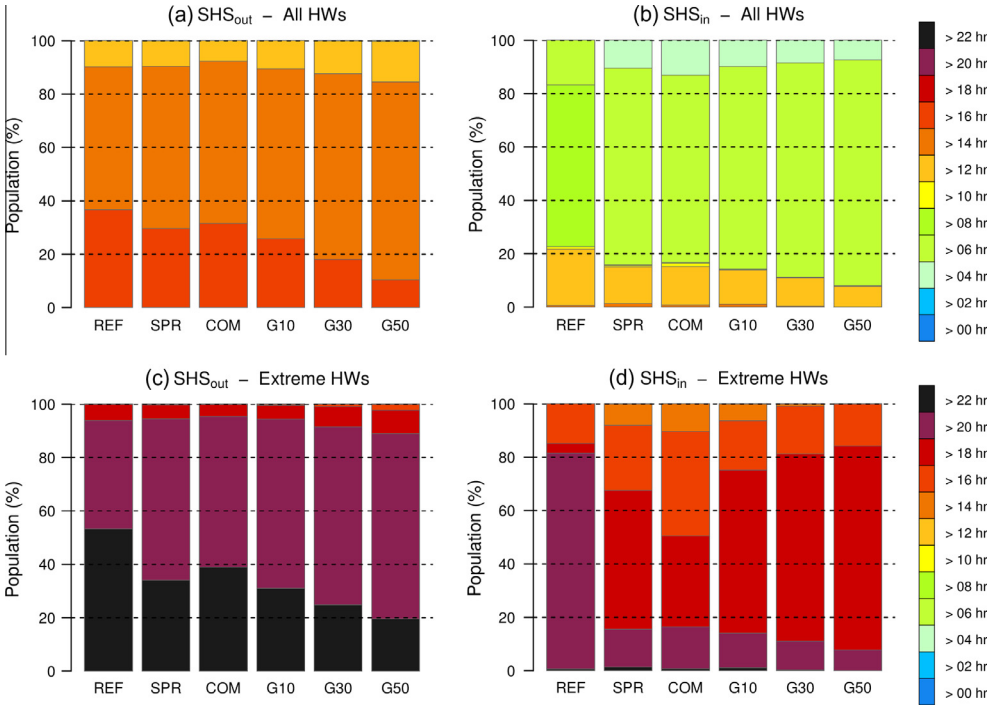

Fig. 14. Distribution of population according to the number of hours per day spent in strong heat stress for outdoor (left) and indoor (right) conditions for the different city scenarios. Results are weighted by the occurrence probabilities of all future heat waves (top) and of the most extreme ones (bottom).

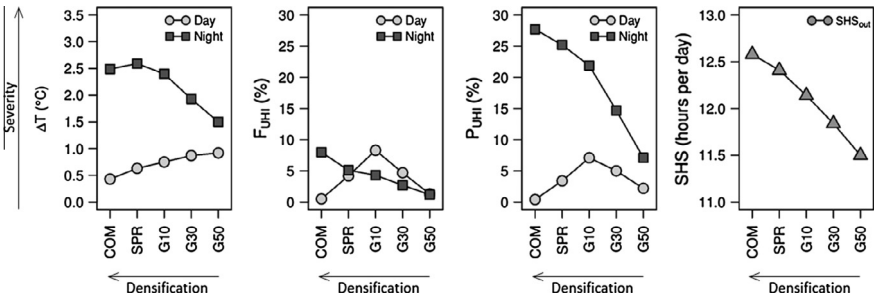

Fig. 15. Example of the indicators computed for the *HW38* event after 14 days for the five scenarios of urban expansion.

of buildings, so that the ambient warms rapidly. Inversely, the best conditions are observed in the multi-family blocks for which the level of renovation is greater. Finally, the residential areas present intermediate conditions. The different trends of urban sprawl have little impacts on indoor thermal comfort which is mostly driven by the quality of buildings' insulation that differs according to building typologies (see details in Appendix A).

The differences noted between scenarios (Fig. 14) are due only to the fact that inhabitants are not distributed identically between collective housing and single housing, whereas the proportion of inhabitants living in the historic city centre is about the same. When the city is more extended, more people occupy single housings and consequently experience more uncomfortable thermal conditions than those living in collective housings.

7. Conclusion

In conclusion, we have tried here to shed new light on how UHI and heat-waves risk can be impacted by different urban planning policies leading to more or less compact urban developments. Using Paris urban area as a case study, five contrasted urban expansion scenarios have been built with the NEDUM-2D model. Due the secular time scale that is investigated here, these scenarios are not an exact and accurate picture of planned policies in Paris. But they illustrate and explore different pathways of urban development strategies. For each of them, the urban climate has been simulated with the physically-based TEB urban canopy model for a large set of heat-wave conditions. Here, different indicators (described in Table 3) are computed in order to measure and investigate UHI effect and heat-wave risk. Fig. 15 shows a summary of the value of these indicators, when computed for the *HW38* event after 14 days.

Whatever the scenario, nocturnal UHI is limited to the most densely built-up areas and reaches up to 2.5–3.0 °C. Inversely, during the day the residential neighbourhoods, which are less protected by the shadow effects, are the warmest places, however in a lesser extend (between 1.0 and 1.5 °C). As a result, the proportion of the city affected by UHI is greater during the day than during the night. However, taking into account the spatial distribution of population in the city brings a different perspective because the city centre is much more populated and consequently more vulnerable. Taking also into account UHI intensity reinforces this message, as UHI amplitude is higher at night than during the day.

Due to UHI, city densification – a strategy widely supported by urban planners and stakeholders – appears to potentially lead to an increased heat wave risk, when compared to urban sprawl. However this conclusion is strongly impacted by the way heat wave risk is measured. In our simulations, the compact city gives rise to the most uncomfortable thermal conditions for outdoor environment, if one takes into account the population repartition in the city and integrate over both days and nights (indicator SHS_{out}). Considering separately days and nights, or not taking into account the population repartition in the city, leads to different messages. This is due to the fact that, whereas the compact city reinforces the UHI at night, it favours solar protection, and therefore cool temperatures during the day.

One of the main results of this study is therefore the qualitatively difference in the messages that one can deduce from UHI simulations, when one consider different UHI or heat wave vulnerability indicators. The impact of a potential urban densification on UHI can either be measured as non-significant (using ΔT indicator), significant but uncertain (using F_{UHI} or P_{UHI} indicators) or strongly negative (using SHS_{out} indicator). The extreme greening of the urban landscape that we analyse here appears significant for all our indicators, sometimes uncertain (using ΔT or F_{UHI} indicator), sometimes strongly positive (P_{UHI} and SHS_{out} indicators).

It is difficult to say which indicator is the most meaningful, and it most certainly depends on the question one wants to answer. Day P_{UHI}, for instance, can be considered of limited interest if people in the city do not stay at home during the day. Favoring F_{UHI} over P_{UHI} also means giving a heavier weight to dense city centre over suburban areas, and this might not necessarily be politically or socially desirable. Considering that the choice of the period and criteria for evaluation is essential, it is consequently tricky to conclude on the most efficient strategy.

The greening of the urban landscape is an interesting option because it generates evapotranspiration while reducing the heat storage process by impervious surfaces. Land availability and water resource are nevertheless major issues in the implementation of such strategies. Their efficiency is dependent on both vegetation density and soil water status (in turn connected with meteorological conditions). In case of long periods of heat waves or hot spells, the benefit of greening strategies is lesser even if vegetation is irrigated.

Our analysis uses simplistic scenarios and hypotheses. Alternative scenarios and indicators are required to get a complete picture. For instance, it would be interesting to consider less extreme city greening scenarios and more extreme densification scenarios. It would also be interesting to repeat our study on other cities, with different sizes and climatic conditions. Other indicators could also be useful to consider, such as for instance potential electric consumption in the case of air conditioning general use in the city, or temperature increase in office districts.

Another important question is whether the differences that we measure here are relevant or not. The differences that we measure between scenarios *COM* and *SPR*, for instance, are small in absolute terms (less than 4% in P_{UHI} and F_{UHI}, 10 min more per day under strong heat stress conditions...). Is such a moderate variation of interest in the policy debate? Addressing this question requires doing a finer analysis of the mechanisms behind our vulnerability to heat, as well as taking into account the costs and obstacles associated with the evolution towards more or less dense urban shapes. These fundamental questions, however, are beyond the scope of this analysis.

Acknowledgments

This study benefited from funding by the French Agency for Research (ANR) through the VURCA project (ANR-08-VULN-013). The authors are grateful to the large VURCA's community, especially Stéphane Hallegatte for initiating the project. They also thank Colette Marchadier and Jean-Luc Salagnac for the elaboration of the database of building characteristics, as well as Anne-Lise Beaulant and Grégoire Pigeon for their contribution to the design and implementation of the modelling platform.

Appendix A. Integrated city scenarios

Within the frameworks of the VURCA project (Hallegatte et al., 2013), integrated city prospective scenarios have been built to translate a possible evolutions of the city at the end of the century. They combine four potential action levers: urban-planning policies to manage the future urban sprawl, adaptation measures for buildings, air-conditioning usage, and watering practices. Each of them consists in different alternatives or hypotheses. In this study, we use the following scenarios.

A.1. Urban sprawl

The urban sprawl is simulated by the NEDUM-2D socio-economic model, forced by macro-economic trends of energy costs especially for oil and demographic pressure (Viguié et al., 2014). NEDUM-2D is a dynamic model which relies on

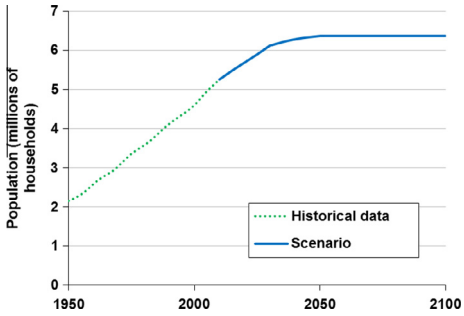

Fig. A1. Demographic scenario used in the simulations.

the classical urban economics framework, an economic modelling approach developed in the end of the 1960s (Alonso, 1964; Mills, 1967; Muth, 1969) which explains the spatial distribution — across the city — of the costs of land and of real estate, housing surface, population density and buildings heights and density. It is based on three main mechanisms.

First, we suppose that households choose their accommodation location and size by making a trade-off between the time and money they spend in transport (i.e. to commute to their jobs) and the real estate price level (or, equivalently, between the proximity to the city centre and the housing surface they can afford). Second, real estate developers choose to build more or less housing (i.e. larger or smaller building) at a specific location, depending on the local level of real estate prices. When these prices are low, developers tend to build low density buildings, and when these prices are high, they tend to build high density buildings. Third, we suppose that various city characteristics do not evolve and adjust at the same speed. For instance, rents can evolve very quickly, whereas buildings change with a much longer timescale. Building depreciation is also very low, leading to path dependency and lockins in city evolution. Using these mechanisms, it is possible to determine the structure of the city from information on population size, households' income, transport network location, building construction costs, and developers behaviour parameters.

The reference scenario (*SPR*) corresponds to the scenario called "SN with high demographic hypothesis" in Viguié et al. (2014). Fig. A1 shows for instance the demographic scenario used in our simulations.

The four other scenarios that we used in this study are identical to this scenario in terms of population evolution, transport prices and people and firms behaviour. Local urban planning policies are however implemented through specific constraints (they are detailed in Section 2.2). Fig. A2 shows simulated city size and green area fraction in the scenarios.

A.2. Buildings characteristics

Four different urban typologies are defined over the study area (see Fig. A3): historic buildings located in the city centre (Haussmannian architecture buildings dating from 19th century), collective housing, single housing, and office buildings. In each grid-cell of the simulation (1 km per 1 km cell), built-up areas in the simulated city can belong to only one of the four classes.

Haussmannian buildings and office buildings are exogenously given: their location are prescribed as input parameters and do not evolve with time. In places where there are no Haussmannian buildings and office buildings, building type is given by buildings floor-area ratio simulated by NEDUM-2D. When this ratio is larger than one, we suppose that building type is collective housing, and when it is lower than one, single housing. In the case of single housing, the respective ground surface devoted to private gardens and to buildings is also computed using this ratio. Simulated population densities and

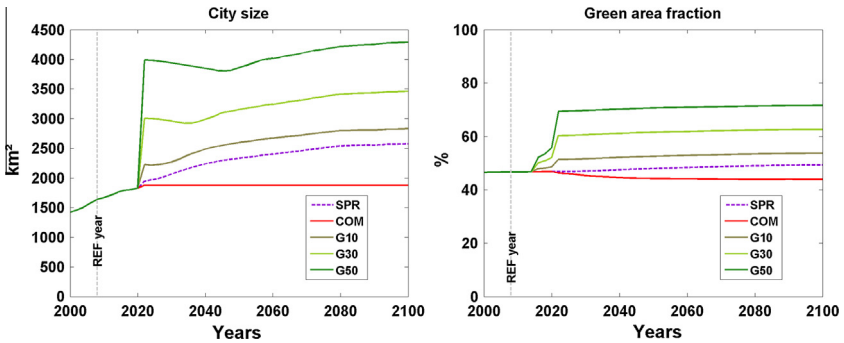

Fig. A2. City size (left) and green area fraction (right) in the scenarios. (For interpretation of the references to colour in this figure legend, the reader is referred to the web version of this article.)

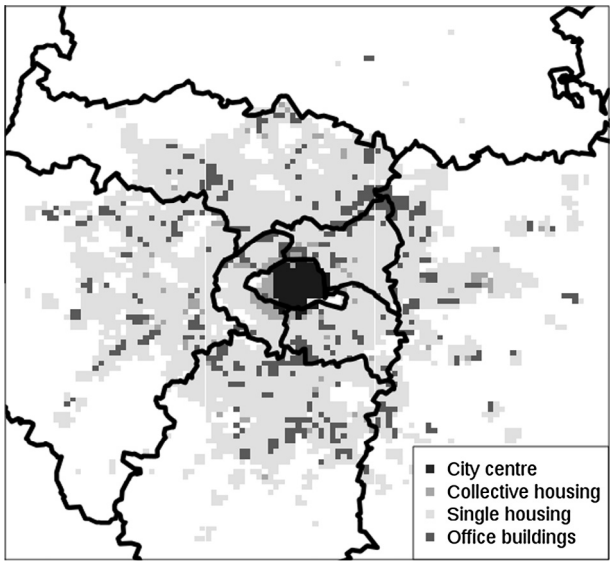

Fig. A3. Typologies of urban landscapes over the study domain, in 2100 in the case of the spread-out city (*SPR*).

floor-area ratio across the city are different in the different scenarios. This makes the total surface devoted to collective housing and to single housing different from one scenario to another. For instance, the denser the city development scenario, the larger the fraction of city surface with collective housing.

Materials characteristics of buildings and renovation techniques are specified differently for each typology on the basis of an inventory of the current Parisian buildings and the renovation trends. Projected buildings characteristics in 2100 are based on the assumption that the energetic performances of buildings are going to improve with time due to the technological progresses in construction and renovation methods, following the current trends. A complete database of buildings characteristics has thus been built within the framework of the VURCA project (Marchadier et al., 2012) and is used here. It is assumed that all collective housing and single housing follow the French thermal regulations fixed by the Grenelle Environmental Forum. The level of renovation is higher for office buildings which are equipped with high-performance vacuum insulation systems and reflective materials. Inversely, because of architectural and aesthetical reasons, the historic buildings are the least renovated ones (a simple interior thermal insulation is implemented in this case).

Appendix B. Building idealized heat waves

The objective of this stage is to produce meteorological conditions over Paris region that represent the future heat waves identified in Section 2.3. These meteorological conditions must be used afterwards to force the TEB urban canopy model. They must consist of hourly spatialized fields of incoming solar and infrared radiation, atmospheric pressure, air temperature, humidity, and wind speed above the top of urban canopy level.

With this aim, a complete three-dimensional atmospheric modelling of the 2003 heat wave (see Step 2 in Fig. 1) is carried out with the Meso-NH non-hydrostatic model (Lafore et al., 1998). The 10th of August 2003 is selected as a reference real case, this being a sunny day with low winds of the 2003 heat wave according to the previous modelling exercises performed by Kounkou-Arnaud et al. (2013) and de Munck et al. (2013). The numerical set-up is time-computing consuming but makes possible to take into account explicitly the retroactions of surface fluxes on the low atmosphere. This reference day of heat wave is consequently run for the today city as well as for each urban expansion scenario. Indeed, the low atmosphere is influenced in different way according to the size, shape, and other characteristics of the city coming from the studied scenarios.

The Meso-NH outputs, required to force TEB, are extracted and stored with a one-hour time step. One single atmospheric level is needed; it is taken 30 m above the top of the urban canopy. These meteorological conditions are then modified and adapted to correspond to different intensities of heat waves. First, the temperature fields provided by Meso-NH are linearly corrected in order to fit the middle value of T_X of each intensity class, i.e. 34, 38, 42, and 46 °C, respectively (see Step 3 in Fig. 1). These heat waves are afterwards referred to as *HW34*, *HW38*, *HW42*, and *HW46*. In order to account for the impact of the temperature modifications on other atmospheric parameters, the specific humidity is recomputed by considering that relative humidity is unchanged; the long-wave incoming radiation is also adjusted to reflect the additional atmospheric emission due to the increase in air temperature. Finally, all these conditions available for one daily cycle are duplicated to build three-week atmospheric forcing.

In the end, meteorological forcing are available for the six city scenarios (including the today city), for the four intensity classes of heat waves, and for events lasting up to three weeks (see Step 3 in Fig. 1). Note that beyond three weeks of heat

wave, a sensitivity study (not presented here) indicates that the local meteorological parameters, especially air temperature in the streets and inside buildings, reach equilibrium or evolve linearly, so that the results can be extrapolated for longer events.

References

Alonso, W., 1964. Location and Land Use. Harvard University Press, Cambridge, MA.

Basara, J.B., Basara, H.G., Illston, B.G., Crawford, K.C., 2010. The impact of the urban heat island during an intense heat wave in Oklahoma City. Adv. Meteorol. http://dx.doi.org/10.1155/2010/230365, Research.

Bass, B., Krayenhoff, E.S., Martilli, A., Stull, R.B., Auld, H., 2003. The impact of green roofs on Toronto's urban heat island. In: Proceedings of the First North American Green Roof Conference: Greening Rooftops for Sustainable Communities, pp. 292–304.

Beniston, M., Stephenson, D., Christensen, O., Ferro, C., Frei, C., et al, 2007. Future extreme events in European climate: an exploration of regional climate model projections. Climatic Change 81 (Suppl. 1), 71–95.

Bröde, P., Fiala, D., Blazejczyk, K., Holmér, I., Jendritzky, G., Kampmann, B., Tinz, B., Havenith, G., 2012. Deriving the operational procedure for the Universal Thermal Climate Index (UTCI). Int. J. Biometeorol. 56, 481–494.

Brueckner, J.K., Largey, A.G., 2008. Social interaction and urban sprawl. J. Urban Econ. 64 (1), 18–34. http://dx.doi.org/10.1016/j.jue.2007.08.002.

Bueno, B., Pigeon, G., Norford, L.K., Zibouche, K., Marchadier, C., 2012. Development and evaluation of a building energy model integrated in the TEB scheme. Geoscientific Model Dev. 5, 433–448.

Chauvin, F., Denvil, S., 2007. Changes in severe indices as simulated by two French coupled global climate models. Global Planet Change 57 (1–2), 96–117.

de Munck, C., 2013. Modélisation de la végétation urbaine et des stratégies d'adaptation au changement climatique pour l'amélioration du confort climatique et de la demande énergétique en ville. PhD Thesis, Paul Sabatier University, Toulouse, France.

de Munck, C., Pigeon, G., Masson, V., Meunier, F., Bousquet, P., Tréméac, B., Merchat, M., Poeuf, P., Marchadier, C., 2013. How much can air conditioning increase air temperatures for a city like Paris, France? Int. J. Climatol. 33 (1), 210–227.

Déqué, M., 2007. Frequency of precipitation and temperature extremes over France in an anthropogenic scenario: model results and statistical correction according to observed values. Global Planet Change 57 (1–2), 16–26.

Eid, J., Overman, H.G., Puga, D., Turner, M.A., 2008. Fat city: questioning the relationship between urban sprawl and obesity. J. Urban Econ. 63 (2), 385–404. http://dx.doi.org/10.1016/j.jue.2007.12.002.

Ewing, R., 1997. Is Los Angeles-style sprawl desirable? J. Am. Plann. Assoc. 63 (1), 107–126.

Ewing, R., Schmid, T., Killingsworth, R., Zlot, A., Raudenbush, S., 2003. Relationship between urban sprawl and physical activity, obesity, and morbidity. Am. J. Health Promot. 18 (1), 47–57.

Fiala, D., Havenith, G., Bröde, P., Kampmann, B., Jendritzky, G., 2012. UTCI-Fiala multi-node model of human heat transfer and temperature regulation. Int. J. Biometeorol. 56, 429–441.

Fujita, M., 1989. Urban Economic Theory: Land Use and City Size. Cambridge University Press, 366pp.

Gabriel, K.M., Endlicher, W.R., 2011. Urban and rural mortality rates during heat waves in Berlin and Brandenburg, Germany. Environ. Pollut. 159 (8-9), 2044–2050. http://dx.doi.org/10.1016/j.envpol.2011.01.016, Epub.

Gordon, P., Richardson, H.W., 1997. Are compact cities a desirable planning goal? J. Am. Plann. Assoc. 63 (1), 95–106.

Hallegatte, S., Viguié, V., Masson, V., Lemonsu, A., Pigeon, G., Beaulant, A.L., Bueno, B., Marchardier, C., Salagnac, J.L., 2013. VURCA Project, Cities Vulnerability to Future Heat Waves & Adaptation Strategies, Final Report, 57pp.

Hamdi, R., Masson, V., 2008. Inclusion of a drag approach in the town energy balance (TEB) scheme: offline 1-d validation in a street canyon. J. Appl. Meteorol. Climatol. 47, 2627–2644.

Hamin, E.M., Gurran, N., 2009. Urban form and climate change: balancing adaptation and mitigation in the U.S. and Australia. Habitat Int. 33 (3), 238–245. http://dx.doi.org/10.1016/j.habitatint.2008.10.005.

Harazono, Y., Teraoka, S., Nakase, I., Ikeda, H., 1991. Effects of rooftop vegetation using artificial substrates on the urban climate and the thermal load of buildings. Energy Build. 15 (3), 435–442.

Huth, R., Kyselý, J., Pokorná, L., 2000. A GCM simulation of heatwaves, dry spells and their relationship to circulation. Climatic Change 46, 29–60.

IPCC, 2013. The Physical Science Basis IPCC Working Group I Contribution to AR5.

Kolokotsa, D., Santamouris, M., Zerefos, S.C., 2013. Green and cool roofs' urban heat island mitigation potential in European climates for office buildings under free floating conditions. Sol. Energy 95, 118–130.

Kounkou-Arnaud, R., Desplat, J., Lemonsu, A., Salagnac, J.L., 2013. Epicea: étude des impacts du changement climatique à Paris. La Météorologie 84, 42–48.

Lafore, J.-P., Stein, J., Asencio, N., Bougeault, P., Ducrocq, V., Duron, J., Fischer, C., Hreil, P., Mascart, P., Masson, V., Pinty, J., Redelsperger, J.L., Richard, E., de Arellano, J.V.G., 1998. The Meso-NH atmospheric simulation system. Part I: adiabatic formulation and control simulation. Ann. Geophys. 16, 90–109. http://dx.doi.org/10.1007/s00585-997-0090-6.

Lambert-Habib, M.L., Hidalgo, J., Fedele, C., Lemonsu, C., Bernard, C., 2013. How is climatic adaptation taken into account by legal tools? Introduction of water and vegetation by French town planning documents. Urban Climate 4, 16–34. http://dx.doi.org/10.1016/j.uclim.2013.04.004.

Lemonsu, A., Grimmond, C., Masson, V., 2004. Modeling the surface energy balance of the core of an old Mediterranean city: Marseille. J. Appl. Meteorol. 43, 312–327.

Lemonsu, A., Masson, V., Shashua-Bar, L., Erell, E., Pearlmutter, D., 2012. Inclusion of vegetation in the Town Energy Balance model for modelling urban green areas. Geoscientific Model Dev. 5, 1377–1393.

Lemonsu, A., Kounkou-Arnaud, R., Desplat, J., Salagnac, J.L., Masson, V., 2013. Evolution of the Parisian urban climate under a global changing climate. Climatic Change 116 (3–4), 679–692. http://dx.doi.org/10.1007/s10584-012-0521-6, Online First, 2012.

Lemonsu, A., Beaulant, A.L., Somot, S., Masson, V., 2014. Evolution of occurrences of heat waves over the Paris basin (France) in the 21st century. Climate Research. http://dx.doi.org/10.3354/cr01235.

Li, D., Bou-Zeid, E., 2013. Synergistic interactions between urban heat islands and heat waves: the impact in cities is larger than the sum of its parts. J. Appl. Meteorol. Climatol. 52, 2051–2064.

Marchadier, C., Pigeon, G., Salagnac, J.-L., 2012. Les scénarios «bâti et usages de la climatisation» et leur simulation (Developing and modeling of scenarios for buildings and air-conditioning usage). Technical note, VURCA research project (available online: http://www.cnrm.meteo.fr/ville.climat/spip.php?action=acceder_document&arg=447&cle=172af20584ccff3f8c8a9ae58c804dde957d6e48&file=pdf%2Fmethodo_scen_bati_v2.0.pdf).

Masson, V., 2000. A physically-based scheme for the urban energy budget in atmospheric models. Bound.-Layer Meteorol. 94, 357–397.

Masson, V., Grimmond, C., Oke, T., 2002. Evaluation of the Town Energy Balance (TEB) scheme with direct measurements from dry districts in two cities. J. Appl. Meteorol. Climatol. 41, 1011–1026.

Masson, V., Lion, Y., Peter, A., Pigeon, G., Buyck, J., Brun, E., 2013a. Grand Paris: regional landscape change to adapt city to climate warming. Climatic Change 117 (4), 769–782. http://dx.doi.org/10.1007/s10584-012-0579-1.

Masson, V., Moigne, P.L., Martin, E., Faroux, S., Alias, A., Alkama, R., Belamari, S., Barbu, A., Boone, A., Bouyssel, F., Brousseau, P., Brun, E., Calvet, J.-C., Carrer, D., Decharme, B., Delire, C., Donier, S., Essaouini, K., Gibelin, A.-L., Giordani, H., Habets, F., Jidane, M., Kerdraon, G., Kourzeneva, E., Lafaysse, M., Lafont, S., Brossier, C.L., Lemonsu, A., Mahfouf, J.-F., Marguinaud, P., Mokhtari, M., Morin, S., Pigeon, G., Salgado, R., Seity, Y., Taillefer, F., Tanguy, G., Tulet, P., Vincendon, B., Vionnet, V., Voldoire, A., 2013b. The SURFEXv7.2 land and ocean surface platform for coupled or offline simulation of Earth surface variables and fluxes. Geoscientific Model Dev. 6, 929–960. http://dx.doi.org/10.5194/gmd-6-929-2013.

McEvoy, D., Lindley, S., Handley, J., 2006. Adaptation and mitigation in urban areas: synergies and conflicts. Proc. Inst. Civil Eng.-Munic. Eng. 159, 185–192.

Meehl, G., Tebaldi, C., 2004. More intense, more frequent, and longer lasting heat waves in the 21st century. Science 305, 994–997.
Mees, H.L.P., Driessen, P.P.J., 2011. Adaptation to climate change in urban areas: climate-greening London, Rotterdam, and Toronto. Climate Law 2 (2), 251–280.
Mills, E.S., 1967. An aggregative model of resource allocation in a metropolitan area. Am. Econ. Rev. 57 (2), 197–210.
Muth, R.F., 1969. Cities and Housing; the Spatial Pattern of Urban Residential Land Use. University of Chicago Press.
Newman, P., Kenworthy, J.R., 1989. Cities and Automobile Dependence: A Sourcebook. Gower Publishing Company, Limited.
Noilhan, J., Planton, S., 1989. A simple parameterization of land surface processes for meteorological models. Mon. Weather Rev. 117, 536–549.
OECD, 2012. Compact city policies: a comparative assessment. Green Growth Studies. OECD. <http://www.oecd.org/gov/regional-policy/compact-city.htm>.
Oke, T.R., 1982. The energetic basis of the urban heat island. Quart. J. Roy. Meteorol. Soc. 108 (455), 1–24.
Pigeon, G., Moscicki, M., Voogt, J., Masson, V., 2008. Simulation of fall and winter surface energy balance over a dense urban area using the TEB scheme. Meteorol. Atmos. Phys. 102 (3–4), 159–171.
Pigeon, G., Zibouche, K., Bueno, B., Le Bras, J., Masson, V., 2014. Improving the capabilities of the Town Energy Balance model with up-to-date building energy simulation algorithms: an application to a set of representative buildings in Paris. Energy Build. 76, 1–14.
Planton, S., Déqué, M., Chauvin, F., Terray, L., 2008. Expected impacts of climate change on extreme climate events. C.R. Geosci. 340, 564–574.
Potchter, O., Cohen, P., Bitan, A., 2006. Climatic behavior of various urban parks during hot and humid summer in the Mediterranean city of Tel Aviv, Israël. Int. J. Climatol. 26 (12), 1695–1711.
Rosenzweig, C., Solecki, W.D., Parshall, L., Lynn, B., Cox, J., Goldberg, R., Hodges, S., Gaffin, S., Slosberg, R.B., Savio, P., et al, 2009. Mitigating New York city's heat island. Bull. Am. Meteorol. Soc. 90 (9), 1297–1312.
Santamouris, M., Synnefa, A., Karlessi, T., 2011. Using advanced cool materials in the urban built environment to mitigate heat islands and improve thermal comfort conditions. Sol. Energy 85, 3085–3102.
Schär, C., Vidale, P., Lüthi, D., Frei, C., Häberli, C., Liniger, M., Appenzeller, C., 2004. The role of increasing temperature variability in European summer heat waves. Nature 427, 332–336.
Schwarz, N., Lautenbach, S., Seppelt, R., 2011. Exploring indicators for quantifying the surface urban heat island with MODIS land surface temperatures. Remote Sens. Environ. 115 (12), 3175–3186.
Shashua-Bar, L., Pearlmutter, D., Erell, E., 2009. The cooling efficiency of urban landscape strategies in a hot dry climate. Landscape Urban Plann. 92 (3–4), 179–186.
Solecki, W.D., Rosenzweig, C., Parshall, L., Pope, G., Clark, M., Cox, J., Wiencke, M., 2005. Mitigation of the heat island effect in urban New Jersey. Global Environ. Change Part B: Environ. Hazards 6 (1), 39–49.
Steeneveld, G.J., Koopmans, S., van Heusinkveld, B.G., Hove, L.W.A., Holtslag, A.A.M., 2011. Quantifying urban heat island effects and human comfort for cities of variable size and urban morphology in the Netherlands. J. Geophys. Res. 116, D20129. http://dx.doi.org/10.1029/2011JD015988.
Stone, B., Rodgers, M.O., 2001. Urban form and thermal efficiency: how the design of cities can influence the urban heat island effect. J.-Am. Plann. Assoc. 67 (2), 186–198.
Streutker, D.R., 2003. Satellite-measured growth of the urban heat island of Houston, Texas. Remote Sens. Environ. 85, 282–289.
Tan, J., Zheng, Y., Tang, X., Guo, C., Li, L., Song, G., Zhen, X., Yuan, D., Kalkstein, A.J., Li, F., Tan, H.C., 2010. The urban heat island and its impact on heat waves and human health in Shanghai. Int. J. Biometeorol. 54, 75–84.
Vautard, R., Yiou, P., D'Andrea, F., de Noblet, N., Viovy, N., Cassou, C., Polcher, J., Ciais, P., Kageyama, M., Fan, Y., 2007. Summertime European heat and drought waves induced by wintertime Mediterranean rainfall deficit. Geophys. Res. Lett. 34, L07711. http://dx.doi.org/10.1029/2006GL028001.
Viguié, V., Hallegatte, S., 2012. Trade-offs and synergies in urban climate policies. Nature Climate Change 2 (5), 334–337. http://dx.doi.org/10.1038/nclimate1434.
Viguié, V., Hallegatte, S., Rozenberg, J., 2014. Downscaling Long term socio-economic scenarios at city scale: a case study on Paris. Technol. Forecast. Soc. Chang. 87, 305–324.
Wong, N., Chen, Y., Ong, C., Sia, A., 2003. Investigation of thermal benefits of rooftop garden in the tropical environment. Build. Environ. 38 (2), 261–270.
Xu, H., Ding, F., Wen, X., 2004. Urban expansion and heat Island dynamics in the Quanzhou region, China. IEEE J. Sel. Top. Appl. Earth Observations Remote Sensing 2 (2), 74–79.